Water-Driven Micromotors

Wei Gao, Allen Pei, and Joseph Wang*

Department of Nanoengineering, University of California, San Diego, La Jolla, California 92093, United States

ABSTRACT

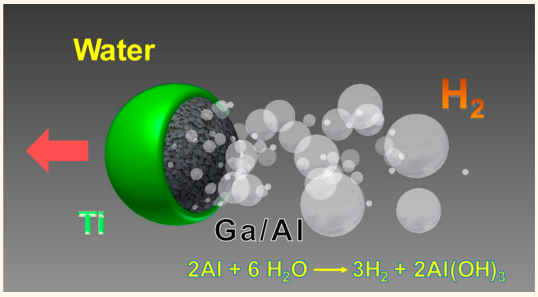

We demonstrate the first example of a water-driven bubble-propelled micromotor that eliminates the requirement for the common hydrogen peroxide fuel. The new water-driven Janus micromotor is composed of a partially coated Al–Ga binary alloy microsphere prepared *via* microcontact mixing of aluminum microparticles and liquid gallium. The ejection of hydrogen bubbles from the exposed Al–Ga alloy hemisphere side, upon its contact with water, provides a powerful directional propulsion thrust. Such spontaneous generation of hydrogen bubbles reflects the rapid reaction between the aluminum alloy and water. The resulting water-driven spherical motors can move at remarkable speeds of 3 mm s^{-1} (*i.e.*, 150 body length s^{-1}), while exerting large forces exceeding 500 pN. Factors influencing the efficiency of the aluminum–water reaction and the resulting propulsion behavior and motor lifetime, including the ionic strength and environmental pH, are investigated. The resulting water-propelled Al–Ga/Ti motors move efficiently in different biological media (*e.g.*, human serum) and hold considerable promise for diverse biomedical or industrial applications.

KEYWORDS: micro/nanomotor · water · propulsion · Janus particles · aluminum–gallium alloy · hydrogen generation

The motion of synthetic microscale objects is of considerable fundamental and practical interest and has thus stimulated major research efforts over the past decade[1−11] in connection to diverse potential applications, ranging from targeted drug delivery[12,13] to environmental remediation.[14] Particular recent attention has been given to chemically powered catalytic nanowires,[2−4] spherical Janus micromotors,[15−17] and tubular microengines[18−22] that exhibit autonomous self-propulsion in the presence of hydrogen peroxide fuel. Unfortunately, the requirement of the hydrogen peroxide fuel greatly impedes many practical applications of catalytically propelled micro/nanoscale motors.[23] Other fuel sources are thus highly desired for diverse real-life applications of nanomotors. Liu and Sen described a Cu–Pt bisegment nanowire motor using dilute aqueous Br_2 or I_2 solutions as the fuel,[24] while Gao *et al.* illustrated acid-driven tubular microengines based on the zinc-induced formation of hydrogen bubbles.[25] Particularly attractive would be new micro/nanomotors that can harvest energy from their own surrounding environment, *i.e.*, use the sample matrix itself as their fuel source, thus obviating the need for adding external fuels. Realizing this important goal will require the identification of new motor compositions and catalytic reactions.

This article describes the first example of a water-driven microscale motor. To accomplish the goal of generating the bubble-thrust essential for an efficient autonomous movement, we have focused here on the water-splitting reaction that generates hydrogen bubbles. One of the promising approaches to produce hydrogen involves the use of aluminum to reduce water to hydrogen:[26−29]

$$2Al(s) + 6H_2O(aq) \rightarrow 2Al(OH)_3(s) + 3H_2(g)$$

However, the utility of this reaction process is strongly hindered by a rapidly formed oxide passivation layer on the Al surface.[29] This problem can be addressed by using aluminum alloys, especially with gallium, indium, or tin.[30−32] In particular, using the Al–Ga system, liquid Ga rapidly penetrates into the solid Al along its grain boundaries in a process known as liquid metal embrittlement.[32] The surface diffusion of Ga is responsible for the removal of the reaction-hindering Al oxide film, thus dramatically promoting the aluminum–water reaction. The presence of such a liquid phase in the alloy microstructure thus leads to a continuous generation of hydrogen, making Al–Ga alloys attractive candidates for designing water-driven micromotors. Unlike violently hydrogen-generating alkali metals, such as sodium and potassium, aluminum alloys offer greater stability and much lower costs.

RESULTS AND DISCUSSION

In order to use the hydrogen-releasing reaction between aluminum alloys and

* Address correspondence to josephwang@ucsd.edu.

Received for review July 23, 2012 and accepted August 14, 2012.

Published online August 14, 2012
10.1021/nn303309z

water, we have designed spherical bubble-propelled Janus micromotors based on coating one side of an Al–Ga microparticle with a titanium layer (Figure 1). The new micromotors have an average diameter of 20 μm and can be propelled at a very high speed of 3 mm s^{-1}, corresponding to 150 body length s^{-1}. Such fast movement reflects the net momentum associated with the detachment of hydrogen bubbles (from the exposed Al–Ga side), which leads to a directional propulsion thrust, analogous to the oxygen-bubble-propelled, peroxide-driven, Pt-based Janus micromotors.[15] In the following sections we will describe the preparation of such water-propelled Al–Ga/Ti Janus microparticles and discuss their locomotion behavior (speed, lifetime, directionality, *etc.*) under different experimental conditions (media, pH, and ionic strength).

The spherical Al–Ga/Ti micromotors were fabricated through the simple sequential process illustrated in Figure 2. Aluminum particles (average size 20 μm) and liquid gallium (at 80 °C) are spread onto separate glass slides at a 1:1 mass ratio (a). The two slides were then pressed and kept together for 1 h at 80 °C, allowing formation of the Al–Ga alloy *via* microcontact mixing (b). During this period, gallium penetrated into the aluminum particles to form the outer alloy layer. The slides were then separated with the Al–Ga microparticles remaining on one of the surfaces (c). Subsequently, one side of the particles was coated with a titanium layer *via* e-beam evaporation to form the asymmetric Janus microstructure (d). After brief sonication in 2-propanol, the micromotors were released from the glass slide and dispersed into 2-propanol (e) for storage until use.

The resulting Janus micromotors were characterized by scanning electron microscope (SEM) and energy-dispersive X-ray spectroscopy (EDX) analysis. The EDX data of Figure 3 illustrate the distribution of gallium, aluminum, and titanium within the Janus spherical micromotor. It indicates that gallium has penetrated into the grain boundaries of the aluminum particle (*via* liquid metal embrittlement), while aluminum has dissolved into the liquid gallium coating, forming an Al–Ga alloy layer over the entire surface. The EDX and SEM data also show that the outer titanium layer covers slightly more than half of the particle, as desired for facilitating the bubble ejection from the opposite (exposed Al–Ga) side and creating a directional propulsion thrust.

X-ray fluorescence analysis was used for estimating the Ga/Al composition ratio of the micromotor. The spectrum of SI Figure 1 indicates mass and atomic Ga/Al ratios of ~3:7 and 14:86, respectively. These ratios correspond to a lower fraction of gallium in the particles than originally used during their preparation, reflecting the gallium portion remaining on the glass slide after the microparticle removal (Figure 2; step d).

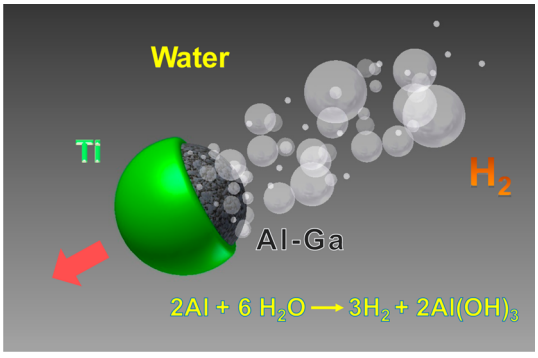

Figure 1. Schematic image of a water-driven hydrogen-propelled Al–Ga/Ti micromotor. The dark hemisphere (right) represents the Al–Ga alloy, while the green area (left) corresponds to the asymmetric Ti coating on one side of the sphere.

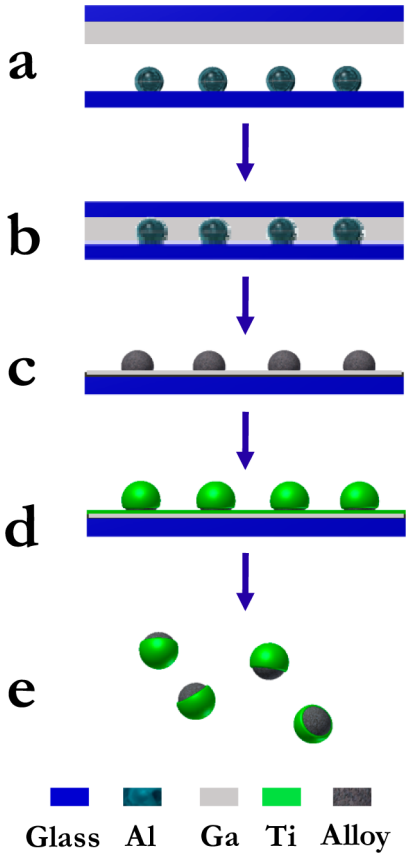

Figure 2. Fabrication of water-driven Al–Ga/Ti micromotors: coating separate slides with liquid gallium and aluminum particles (a), alloy formation by microcontact mixing of the aluminum particles and "liquid" gallium (b), detachment of the slides (c), coating one side of the Al–Ga particles with a Ti layer by e-beam evaporation (d), and separation of the individual micromotors by sonication in 2-propanol (e).

Figure 4 illustrates the ultrafast propulsion of an Al–Ga/Ti micromotor in ultrapure water. It shows time-lapse images, taken from SI Video 1, over a 300 ms period. A long tail of hydrogen bubbles generated on one side of the micromotor is clearly observed,

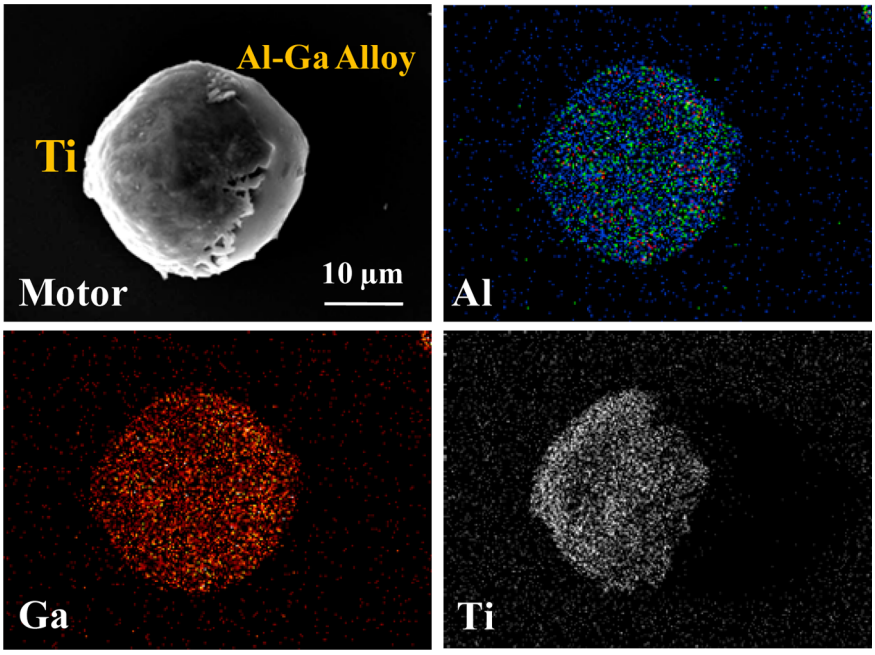

Figure 3. Scanning electron microscope (SEM) image and energy-dispersive X-ray (EDX) spectroscopy results showing the distribution of Ga, Al, and Ti in the Janus Al−Ga/Ti micromotor.

reflecting the rapid spontaneous reaction of aluminum with the surrounding water. The average diameter of these ejected hydrogen bubbles is around 10 μm. The fast production of small bubbles and the steady motor propulsion are also clearly illustrated in the corresponding video. Such bubble generation imparts the strong momentum that propels the micromotor forward in a relatively straight path. This leads to a remarkable speed of 3 mm s^{-1}, which corresponds to 150 body length s^{-1}. This represents a very large drive force of over 500 pN, based on the drag force for a spherical colloid (equals the drive force), $F = 6\pi\mu av$, where a is the radius of the sphere, v is the speed of the micromotor, and μ is the viscosity of water.[15] Such speed and force are significantly higher than those reported for common (peroxide-driven) catalytic Janus particles.[15−17]

Various control experiments, illustrated in Figure 5 and corresponding SI Video 2, were used to demonstrate the crucial roles of the "liquid" phase of the Al−Ga microparticles and of the sputtered Ti layer in the observed directional propulsion. For example, no bubble generation is observed in Figure 5a for the plain Al microparticle, as the presence of an oxide passivation layer (expected in the absence of Ga) hinders the Al reaction with water.[30,31] Similarly, no directional movement is observed in Figure 5b and SI Video 2 for an Al−Ga alloy particle, without the partial Ti coating, owing to the symmetric generation of numerous hydrogen bubbles from the entire surface. In contrast, a clear directed movement is observed in Figure 5c for the partially covered microparticle, reflecting the asymmetric bubble generation associated with the effectiveness of the Ti layer in blocking the aluminum−water reaction.

The liquid phase of the Al−Ga particles—essential for the aluminum−water reaction[32,33]—is readily obtained by heating the particles during the preparation process (described previously), as the melting point of the resulting alloy is lower than room temperature.[33] This liquid phase of the Al−Ga alloy is developed when small amounts of solid Al dissolve into the liquid Ga occupying the outer particle layer. It is this solvated Al, present in the liquid phase, that reacts readily with water[32] at the motor−solution interface, generating hydrogen bubbles. As this localized Al is dissolved and depleted during the reaction, additional Al from the interior solid part dissolves into the outer Ga layer to restore the liquid-phase equilibrium. Eventually, this process depletes the solid Al at the center of the particle. The generation and ejection of the hydrogen bubbles leads to the removal of the passivating $Al(OH)_3$ layer formed at the surface of the liquid phase. The melting point of the Al−Ga alloy depends on the specific Al/Ga ratio in the particle; for the Al/Ga ratio employed in this study, the alloy remains in the liquid phase at room temperature,[33] which is essential for the aluminum−water reaction and continuous motor operation.

The micromotors maintain a similar propulsion behavior (with a speed of around 3 mm/s) in weak acid or base solutions of pH values ranging from pH 4 to pH 10, reflecting the fact that these media have a limited effect upon the efficiency of the aluminum−water reaction.[34] However, in strongly acidic or alkaline media (pH < 2 or pH > 12, respectively), different

hydrogen generation reactions take place, reflecting the amphoteric properties of the aluminum and aluminum oxide.[35] It is well-established that strong acids and bases are able to destroy the protective oxide layer on the aluminum surface to facilitate different hydrogen generation pathways.[35] This is also supported by additional experiments illustrating significantly longer motor lifetimes (of over 5 min) in pH 0 or pH 14 compared to the limited lifetime and hydrogen yield observed under mild environments.

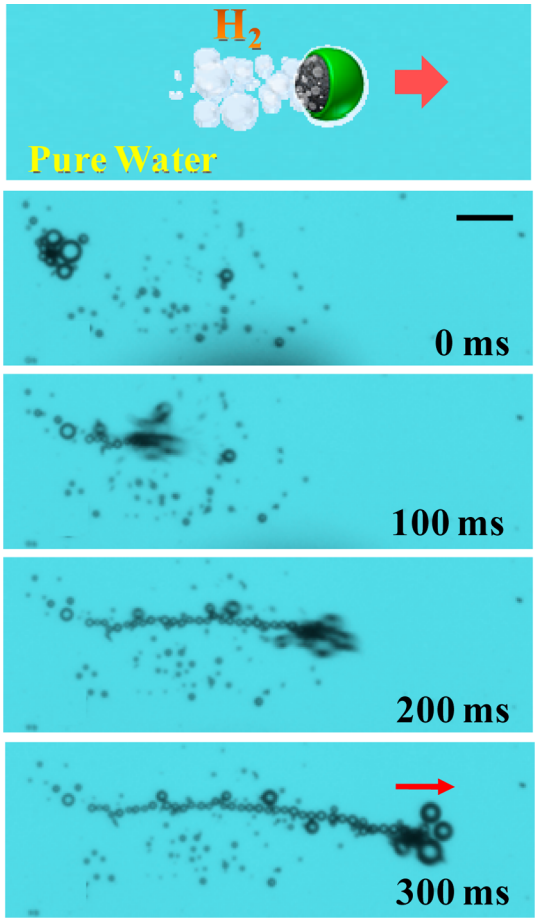

Figure 4. Water-driven Al–Ga/Ti micromotor: time-lapse images, taken from SI Video 1, illustrating the motor propulsion at 0, 100, 200, and 300 ms intervals. Scale bar: 100 μm. Medium: ultrapure water containing 0.05% Triton X-100.

The influence of the salt (chloride ion) concentration upon the water-driven movement was also examined. Figure 6 illustrates the motion of the Al–Ga/Ti micromotor in sodium chloride solutions of different concentrations (10–1000 mM). These images clearly indicate that the efficiency of the micromotors decreases as the salt concentration increases. Accordingly, the speed of the micromotor is reduced from 3000 μm s^{-1} without the salt to 1300 and 100 μm s^{-1} in 10 mM and 1 M NaCl solutions, respectively. The increased salt concentration leads to a lower bubble frequency and a larger bubble size, reflecting the lower reaction rate (*i.e.*, slower Al dissolution) in the salt-rich media. As expected,[21] such larger bubble size and lower frequency lead to a slower propulsion speed. The slower hydrogen evolution at higher NaCl concentrations leads also to longer motor lifetimes of up to 5 min. It has been shown that chloride ions readily penetrate the oxide layer formed on the Al surface upon contact with water, resulting in local Al dissolution (under the oxide film) through a pitting corrosion process.[29,36,37] The pitting corrosion of Al leads to "blisters" that fill with hydrogen gas and water as they rupture. As illustrated in SI Figure 2b and the corresponding SI Video 4, the Al–Ga/Ti micromotor can move even in a 3 M sodium chloride solution at a speed of 45 μm s^{-1} without adding any surfactant. In contrast, no obvious bubble generation and movement are observed upon exposing Janus Al/Ti microparticles (without Ga) to 3 M sodium chloride (SI Figure 2a). In addition, no obvious movement was observed using the Al–Ga/Ti microparticle in sodium sulfate solutions (containing more than 0.5 M salt), reflecting the inhibited aluminum–water reaction by sulfate ions (compared to the chloride ions).[38]

The lifetime of the Al–Ga micromotor can range from a few minutes down to a few seconds, depending on the size of the Al particle, surrounding solution, temperature, and preparation process, which influence

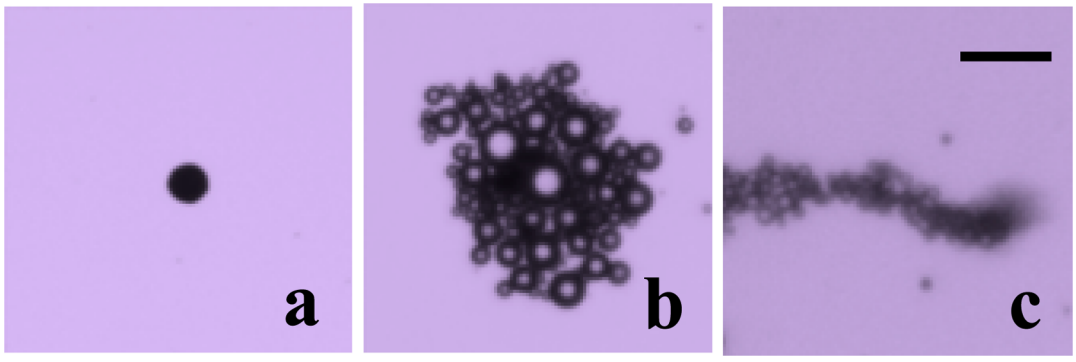

Figure 5. Control experiments (taken from SI Video 2) using an Al microparticle (a) and an uncoated Al–Ga alloy microparticle (b) compared to an Al–Ga/Ti micromotor (c). Media: pure water with 0.1% Triton X-100. Scale bar: 50 μm.

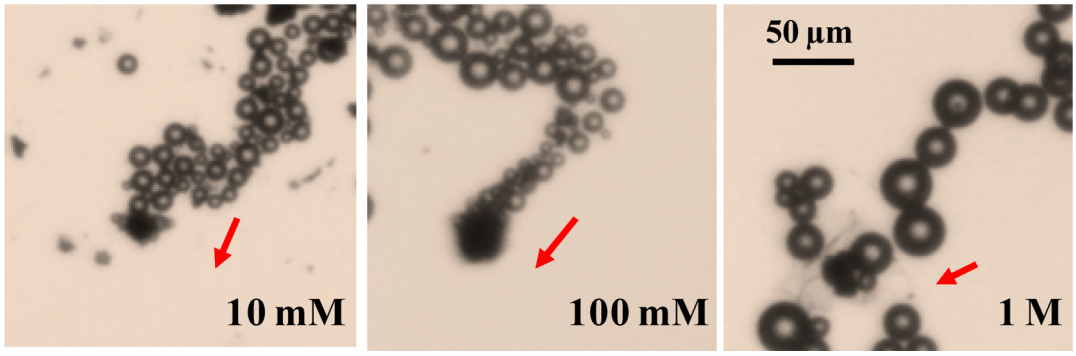

Figure 6. Influence of the salt (sodium chloride) concentration upon the propulsion of the Al–Ga/Ti micromotor. Images taken from the corresponding SI Video 3. Conditions: as in Figure 5c.

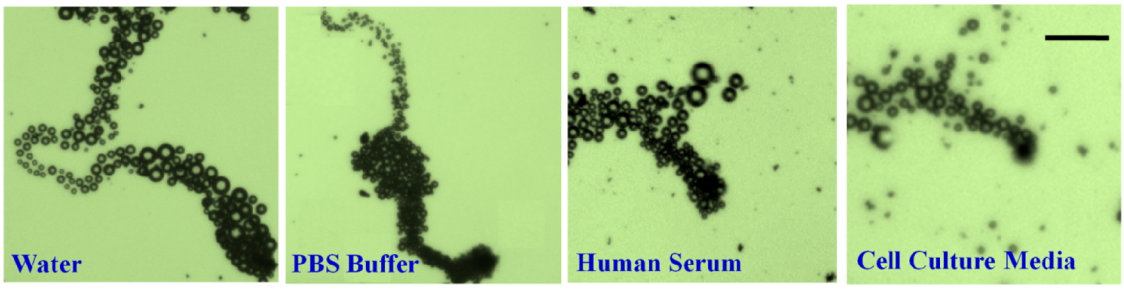

Figure 7. Movement of Al–Ga/Ti micromotors in various media: water, PBS buffer (pH 7.0), human serum, and cell culture medium (taken from SI Video 5). Scale bar: 100 μm. Conditions: as in Figure 5c.

the aluminum–water reactivity and Al mass. For example, the longer lifetime of 5 min was observed in 3 M sodium chloride solutions using 20 μm diameter Al–Ga/Ti microparticles prepared by alloying the Al for one week (to increase the amount of Al involved in the hydrogen generation[32]). Additional parameters, such as the temperature, Al grain size, strain rate, stress, and exposure time to the liquid metal prior to testing, could also influence the reaction efficiency and lifetime of Al–Ga/Ti micromotors.

The new Al–Ga alloy micromotor can operate in different environments. For example, the images in Figure 7 (along with SI Video 5) illustrate the efficient propulsion of the new micromotors in pure water, phosphate buffer saline (PBS) buffer, human serum, and cell culture media. The speed decreased from 3 mm s^{-1} in pure water to 1200, 600, and 500 μm s^{-1} in the cell culture media, PBS, and human serum, respectively. Such slower speeds reflect the increased environmental viscosity in these media. Protein fouling of the motor surface may also contribute to the substantially slower speed observed in human serum. Yet, even the slowest speed (observed in serum) corresponds to a very high relative speed of 15 body lengths s^{-1}. This efficient locomotion in various biological media holds great promise for future practical applications.

Further improvements in the propulsion of Al-based alloy motors are expected by replacing the current binary Al–Ga alloy with ternary Al–Ga–In or quaternary Al–Ga–In–Sn alloys. The total percent hydrogen-gas yield increases sharply from 3–8% (for the Al–Ga alloy) to around 80% (using Al–Ga–In–Sn), reflecting a higher Al fraction involved in the reaction.[32] Such efficient gas generation would allow the water-driven motor to sustain movement over extended periods. The lower hydrogen yield of the binary alloy is consistent with the observations of short motor lifetimes (of less than a minute) in pure water, as only a very small portion of the motor is involved in the reaction with water. Additional experiments have thus been performed toward micromotors based on the ternary Al–Ga–In alloy. Yet, because of the high reactivity and low stability of the Al–Ga–In alloy, the microparticles reacted with the water vapor in the air immediately after their preparation. Such fast reaction could be clearly observed by a gradual color change of the particles and from the growth of oxide microstructures on the particle surfaces. The reaction of these water-vapor-exposed Al–Ga–In/Ti particles in aqueous medium lasted over two minutes, compared to Al–Ga/Ti particles, reflecting the overall higher hydrogen yield of the ternary alloy. Preparing and storing ternary or quaternary alloy micromotors in an inert environment should lead to more sustained motor lifetimes.

CONCLUSIONS

We have presented the first example of chemically powered micromotors propelled autonomously using water as the sole fuel source. While the water-splitting reaction was used before to drive bipolar-electrochemical

macroscale motors under an external electrical field,[10] it has not been used for the locomotion of self-propelled chemically powered micromotors. The water-splitting reaction, involving Al–Ga alloys, has been used for realizing such water-driven microscale motion, with the reaction and propulsion efficiencies improving *via* the liquid metal embrittlement in the Al–Ga system. The presence of such a liquid phase in the alloy microstructure facilitates the continuous hydrogen-generating reaction between aluminum and water. We have demonstrated that the resulting water-driven Al–Ga/Ti micromotors can swim in water at 150 body lengths per second, as well as in biological media such as human serum. Further improvements in the propulsion behavior are expected by enhancing the alloy reactivity *via* a judicious control of its microstructure and composition. New water-splitting catalytic reactions and materials, offering extended motor lifetimes and/or higher efficiency, are also highly desired for future water-driven nanomotor operations. The new water-driven motion capability should greatly expand the scope of applications and environments of chemically powered nanomachines. In particular, these water-driven micromotors could have a profound impact on diverse biomedical or industrial applications of micromotors, ranging from targeted drug delivery to microchip diagnostics, where the use of the common peroxide fuel is not desirable or possible.

EXPERIMENTAL SECTION

Synthesis of Al–Ga/Ti Micromotors. The micromotors were prepared using aluminum microparticles (average 20 μm size, Alpha Chemicals, Hollister, MO, USA) as the base particles. Aluminum particles were spread onto a glass slide, while gallium (catalog #263265, Sigma-Aldrich, St Louis, MO, USA) was melted at 80 °C and spread onto another glass slide, at a level corresponding to a mass ratio of 1:1 (Al:Ga). The two slides were pressed together and mixed until the particles were evenly distributed and well-coated. Then, the particles were kept for 1 h at 80 °C. The alloy particles were coated with a titanium layer at 2.5 Å/s for 200 nm using a Temescal BJD 1800 e-beam evaporator under a pressure of 1×10^{-7} Torr. After sonicating the slides briefly in 2-propanol, the micromotors were released from the glass slide and dispersed into 2-propanol. The motors were stored in the pure 2-propanol solution until use. This process leads to a relatively high yield, with more than 75% of particles displaying efficient bubbling in water. Aluminum–gallium–indium alloy particles were prepared using a similar protocol but using gallium–indium eutectic (catalog #495425, Sigma-Aldrich).

Reagents and Solutions. Ultrapure water (18.2 MΩ·cm), containing 0.05–0.1% Triton X-100 (Fisher Scientific, Fair Lawn, NJ, USA), was used as propulsion media in most experiments. Experiments in human serum samples were carried out by mixing 0.2% Triton solution and human serum (from human male AB plasma) (Sigma-Aldrich) at a 1:1 ratio. Experiments involving PBS (pH 7.0) and cell culture media (catalog no. 15-040-CV, Mediatech Inc., Manassas, VA, USA) were carried out in pure media containing 0.1% Triton X-100.

Equipment. Scanning electron microscopy images were obtained with a Phillips XL30 ESEM instrument, using an acceleration potential of 20 kV. The micromotors are characterized using EDX analysis (Oxford EDX attachment and Inca software in ESEM) and by X-ray fluorescence spectroscopy (Horiba XGT-5000 X-ray analytical microscope). Videos were captured by an inverted optical microscope (Nikon Instrument Inc. Ti-S/L100), coupled with 10× and 5× objectives, and a Hamamatsu digital camera C11440 using the NIS-Elements AR 3.2 software.

Conflict of Interest: The authors declare no competing financial interest.

Supporting Information Available: Additional figures, data, and videos. This material is available free of charge *via* the Internet at http://pubs.acs.org.

Acknowledgment. This work was supported by the National Science Foundation (no. CBET 0853375) and the United States Department of Energy (grant no. DE-SC0004937). The authors also thank S. Sattayasamitsathit and A. Katzenberg for their help.

REFERENCES AND NOTES

1. Ismagilov, R. F.; Schwartz, A.; Bowden, N.; Whitesides, G. M. Autonomous Movement and Self-Assembly. *Angew. Chem., Int. Ed.* **2002**, *41*, 652–654.
2. Paxton, W. F.; Kistler, K. C.; Olmeda, C. C.; Sen, A.; St. Angelo, S. K.; Cao, Y.; Mallouk, T. E.; Lammert, P. E.; Crespi, V. H. Catalytic Nanomotors: Autonomous Movement of Striped Nanorods. *J. Am. Chem. Soc.* **2004**, *126*, 13424–13431.
3. Fournier-Bidoz, S.; Arsenault, A. C.; Manners, I.; Ozin, G. A. Synthetic Self-Propelled Nanomotors. *Chem. Commun.* **2005**, 441–443.
4. Mallouk, T. E.; Sen, A. Powering Nanorobots. *Sci. Am.* **2009**, *300*, 72–77.
5. Wang, J. Can Man-Made Nanomachines Compete with Nature Biomotors? *ACS Nano* **2009**, *3*, 4–9.
6. Mirkovic, T.; Zacharia, N. S.; Scholes, G. D.; Ozin, G. A. Fuel for Thought: Chemically Powered Nanomotors Out-Swim Nature's Flagellated Bacteria. *ACS Nano* **2010**, *4*, 1782–1789.
7. Sanchez, S.; Pumera, M. Nanorobots: The Ultimate Wireless Self-Propelled Sensing and Actuating Devices. *Chem. –Asian J.* **2009**, *4*, 1402–1410.
8. Zhang, L.; Abbott, J. J.; Dong, L.; Peyer, K. E.; Kratochvil, B. E.; Zhang, H.; Bergeles, C.; Nelson, B. J. Characterizing the Swimming Properties of Artificial Bacterial Flagella. *Nano Lett.* **2009**, *9*, 3663–3667.
9. Gao, W.; Sattayasamitsathit, S.; Manesh, K. M.; Weihs, D.; Wang, J. Magnetically Powered Flexible Metal Nanowire Motors. *J. Am. Chem. Soc.* **2010**, *132*, 14403–14405.
10. Loget, G.; Kuhn, A. Electric Field-Induced Chemical Locomotion of Conducting Objects. *Nat. Commun.* **2011**, *2*, 10.1038/ncomms1550.
11. Loget, G.; Kuhn, A. Propulsion of Microobjects by Dynamic Bipolar Self-Regeneration. *J. Am. Chem. Soc.* **2010**, *132*, 15918–15919.
12. Zhang, L.; Petit, T.; Peyer, K. E.; Nelson, B. J. Targeted Cargo Delivery Using a Rotating Nickel Nanowire. *Nanomed.-Nanotechnol. Biol. Med.* **2012**, 10.1016/j.nano.2012.03.002.
13. Gao, W.; Kagan, D.; Pak, O. S.; Clawson, C.; Campuzano, S.; Chuluun-Erdene, E.; Shipton, E.; Fullerton, E. E.; Zhang, L.; Lauga, E.; *et al.* Cargo-Towing Fuel-Free Magnetic Nanoswimmers for Targeted Drug Delivery. *Small* **2012**, *8*, 460–467.
14. Guix, M.; Orozco, J.; Garcia, M.; Gao, W.; Sattayasamitsathit, S.; Merkoci, A.; Escarpa, A.; Wang, J. Superhydrophobic Alkanethiol-Coated Microsubmarines for Effective Removal of Oil. *ACS Nano* **2012**, *6*, 4445–4451.
15. Gibbs, J. G.; Zhao, Y.-P. Autonomously Motile Catalytic Nanomotors by Bubble Propulsion. *Appl. Phys. Lett.* **2009**, *94*, 163104.
16. Howse, J. R.; Jones, R. A.; Ryan, A. J.; Gough, T.; Vafabakhsh, R.; Golestanian, R. Self-Motile Colloidal Particles: from

Directed Propulsion to Random Walk. *Phys. Rev. Lett.* **2007**, *99*, 048102.
17. Baraban, L.; Makarov, D.; Streubel, R.; Monch, I.; Grimm, D.; Sanchez, S.; Schmidt, O. G. Catalytic Janus Motors on Microfluidic Chip: Deterministic Motion for Targeted Cargo Delivery. *ACS Nano* **2012**, *6*, 3383–3389.
18. Mei, Y. F.; Huang, G. S.; Solovev, A. A.; Urena, E. B.; Monch, I.; Ding, F.; Reindl, T.; Fu, R. K. Y.; Chu, P. K.; Schmidt, O. G. Versatile Approach for Integrative and Functionalized Tubes by Strain Engineering of Nanomembranes on Polymers. *Adv. Mater.* **2008**, *20*, 4085–4090.
19. Solovev, A. A.; Mei, Y. F.; Urena, E. B.; Huang, G. S.; Schmidt, O. G. Catalytic Microtubular Jet Engines Self-Propelled by Accumulated Gas Bubbles. *Small* **2009**, *5*, 1688–1692.
20. Manesh, K. M.; Yuan, R.; Clark, M.; Kagan, D.; Balasubramanian, S.; Wang, J. Template-Assisted Fabrication of Salt-Independent Catalytic Tubular Microengines. *ACS Nano* **2010**, *4*, 1799–1804.
21. Gao, W.; Sattayasamitsathit, S.; Orozco, J.; Wang, J. Highly Efficient Catalytic Microengines: Template Electrosynthesis of Polyaniline/Platinum Microtubes. *J. Am. Chem. Soc.* **2011**, *133*, 11862–11864.
22. Huang, G. S.; Wang, J.; Mei, Y. F. Material Considerations and Locomotive Capability in Catalytic Tubular Microengines. *J. Mater. Chem.* **2012**, *22*, 6519–6525.
23. Wang, J.; Gao, W. Nano/Microscale Motors: Biomedical Opportunities and Challenges. *ACS Nano* **2012**, *6*, 5745–5751.
24. Liu, R.; Sen, A. Autonomous Nanomotor Based on Copper–Platinum Segmented Nanobattery. *J. Am. Chem. Soc.* **2011**, *133*, 20064–20067.
25. Gao, W.; Uygun, A.; Wang, J. Hydrogen-Bubble-Propelled Zinc-Based Microrockets in Strongly Acidic Media. *J. Am. Chem. Soc.* **2012**, *134*, 897–900.
26. Soler, L.; Macanás, J.; Muñoz, M.; Casado, J. Aluminum and Aluminum Alloys as Sources of Hydrogen for Fuel Cell Applications. *J. Power Sources* **2007**, *169*, 144–149.
27. Wang, H. Z.; Leung, D. Y. C.; Leung, M. K. H.; Ni, M. Enhancement of Hydrogen Generation Rate in Reaction of Aluminum with Water. *Renew. Sustain. Energy Rev.* **2009**, *13*, 845–853.
28. Roach, P. J.; Woodward, W.; Castleman, A. W., Jr.; Reber, A. C.; Khanna, S. N. Complementary Active Sites Cause Size-Selective Reactivity of Aluminum Cluster Anions with Water. *Science* **2009**, *323*, 492–495.
29. Szklarska-Smialowska, Z. Pitting Corrosion of Aluminum. *Corros. Sci.* **1999**, *41*, 1743–1767.
30. Flamini, D. O.; Saidman, S. B.; Bessone, J. B. Aluminium Activation Produced by Gallium. *Corros. Sci.* **2006**, *48*, 1413–1425.
31. Kravchenko, O. V.; Semenenko, K. N.; Bulychev, B. M.; Kalmykov, K. B. Activation of Aluminum Metal and its Reaction with Water. *J. Alloys Compd.* **2005**, *397*, 58–62.
32. Ziebarth, J. T.; Woodall, J. M.; Kramer, R. A.; Choi, G. Liquid Phase-Enabled Reaction of Al-Ga and Al-Ga-In-Sn Alloys with Water. *Int. J. Hydrogen Energy* **2011**, *36*, 5271–5279.
33. Baker, H. *ASM_Handbook, Alloy Phase Diagrams*; ASM International: Materials Park, OH, 1992; Vol. 3.
34. Kolics, A.; Besing, A. S.; Baradlai, P.; Haasch, R.; Wieckowski, A. Effect of pH on Thickness and Ion Content of the Oxide Film on Aluminum in NaCl Media. *J. Electrochem. Soc.* **2001**, *148*, B251–B259.
35. Birnbaum, H. K.; Buckley, C.; Zeides, F.; Sirois, E.; Rozenak, P.; Spooner, S.; Lin, J. S. Hydrogen in Aluminum. *J. Alloys Compd.* **1997**, *253–254*, 260–264.
36. Czech, E.; Troczynski, T. Hydrogen Generation through Massive Corrosion of Deformed Aluminum in Water. *Int. J. Hydrogen Energy* **2010**, *35*, 1029–1037.
37. McCafferty, E. Sequence of Steps in the Pitting of Aluminum by Chloride Ions. *Corros. Sci.* **2003**, *45*, 1421–1438.
38. Pyun, S. I.; Moon, S. M. The Inhibition Mechanism of Pitting Corrosion of Pure Aluminum by Nitrate and Sulfate Ions in Neutral Chloride Solution. *J. Solid State Electrochem.* **1999**, *3*, 331–336.